Hindawi Publishing Corporation
Mathematical Problems in Engineering
Volume 2015, Article ID 632912, 9 pages
http://dx.doi.org/10.1155/2015/632912

Research Article

Prediction of Load Capacity Variation in FRP Bonded Concrete Specimens Using Brownian Motion

Tayyebeh Mohammadi,[1] Baolin Wan,[1] Jian-Guo Dai,[2] and Chao Zhu[3]

[1]*Department of Civil, Construction, and Environmental Engineering, Marquette University, P.O. Box 1881, Milwaukee, WI 53201-1881, USA*
[2]*Department of Civil and Environmental Engineering, The Hong Kong Polytechnic University, Hung Hom, Kowloon, Hong Kong*
[3]*Department of Mathematical Sciences, University of Wisconsin-Milwaukee, P.O. Box 413, Milwaukee, WI 53201-0413, USA*

Correspondence should be addressed to Baolin Wan; baolin.wan@marquette.edu

Received 25 November 2014; Accepted 4 March 2015

Academic Editor: Alejandro Ortega-Moñux

In wet lay-up process, dry fiber sheets are saturated with a polymer and applied to the concrete surface by hand. This causes relatively large variation in properties of the cured FRP composite material. It is hard to know the exact mechanical properties of the FRP constructed by wet lay-up process. In addition, the stiffness of FRP changes during debonding process due to different amount of concrete attached to the debonded FRP at different locations. It is also inevitable to have considerable variations in the strength of concrete. Therefore, the behaviour of FRP bonded concrete members varies among specimens even when the same materials are used. The variation of localized FRP stiffness and concrete strength can be combined in a single parameter as variation of the localized interfacial fracture energy. In an effort to effectively model the effects of the variation of interfacial fracture energy on the load versus deflection responses of FRP bonded concrete specimens subjected to Mode I and Mode II loading, a random white noise using a one-dimensional standard Brownian motion is added to the governing equations, yielding stochastic differential equations. By solving these stochastic equations, the bounds of load carrying capacity variation with 95% probability are found for different experimental tests.

1. Introduction

Extensive research has clearly shown that externally bonded fiber reinforced polymer (FRP) composites have good potential for use in strengthening of concrete members [1–3]. The stiffness of FRP and compressive concrete strength are the most effective parameters on the responses and behaviour of strengthened concrete members [4–6]. However, there are some variations in FRP stiffness (bending stiffness and tension stiffness; hereafter called "stiffness" only unless the tension or bending stiffness needs to be emphasized) and concrete strength, particularly the localized strength. In the following, the sources of the FRP stiffness and concrete strength variations are briefly explained, respectively.

One of the common methods to use FRP to strengthen existing concrete structures is wet lay-up bonding that consists of installation by hand using unidirectional dry fiber sheets or fabrics impregnated with a saturating resin on-site [3]. Since it is hard to accurately determine Young's modulus of the cured FRP constructed by wet lay-up process and there is variation of the cured FRP thickness, it is almost impossible to obtain the accurate magnitude of the FRP stiffness. Generally, the manufacturers provide the properties of the fiber sheets, such as Young's modulus and design sheet thickness, based on the tests in laboratories. However, when it is used in field, the properties of the FRP are affected by the curing process and defects such as gouges or deep scratches which may occur through the instalment of FRP [7, 8]. Typically it is difficult to get the same level of quality control for wet lay-up FRP as for the FRP plates or strips precured in the factory. Therefore, this operation may cause differences between what is in the manufacturer's reports and the actual FRP stiffness achieved *in situ*. The FRP properties may also be dissimilar at different locations even in the same specimen

because the fibers may be curved to different extents at different locations.

Existing experimental studies have shown that in the vast majority of cases, except when a weak adhesive or a high strength concrete is used, debonding failure of an FRP-concrete bonded joint is due to the fracture within the concrete at a small distance from the concrete-adhesive interface [9, 10]. During the debonding failure, the concrete crack path continuously changes direction and the thickness of substrate concrete layer attached to the FRP varies at different locations [11]. This phenomenon causes the stiffness variation during debonding propagation.

Concrete is a mixture of water, cement, sand, aggregate, admixtures, and air. Variations in the properties or proportions of these constituents as well as variations in the transporting, placing, compaction, and curing of the concrete lead to variations in the strength of the finished concrete. In addition, discrepancies in the tests will also cause apparent differences in strength [12]. The concrete near the top of concrete members tends to be weaker than the concrete lower down, probably because of increased water to cement ratio at the top due to upward water migration after the concrete is placed and by greater compaction of concrete near the bottom due to the sinking of aggregates in the form during vibration [13]. Therefore, there is variation of concrete strength at different spots even in the same member.

Since FRP stiffness and concrete strength play important roles in predicting the load carrying capacity and failure modes in FRP-strengthened concrete members, it is useful to find a way to determine the range of actual values of FRP stiffness and concrete strength without testing each of them. Since the fracture energy is a function of concrete strength and FRP stiffness in FRP concrete bonds [6], FRP stiffness and concrete strength variations can combine together as the interfacial fracture energy variation. In this study, the concepts of Brownian motion and white noise from probability theory are used to find the fracture energy range instead of variations of the FRP stiffness and concrete strength separately.

Brownian motion is the macroscopic picture emerging from a particle moving randomly in d-dimensional space. The term "Brownian motion" can also refer to the mathematical model used to define such random movements. If just one direction for the movements in an instant of time is assumed, then it is named one-dimensional Brownian motion. White noise generally is a random signal that can be applied to model a totally unpredictable process. It can be considered as the derivative of a Brownian motion existing in the stationary sense. In the next section, Brownian motion and white noise will be introduced briefly.

In this study, a random white noise is added to the fracture energy parameter in the governing equations to model fluctuating differences between actual and theoretical values of FRP stiffness and concrete strength. The governing equations for FRP debonding from concrete subjected to Mode I (normal stress perpendicular to the interface) and Mode II (in-plane shear stress parallel to the interface) loadings become stochastic differential equations, where the driven noise is a one-dimensional standard Brownian motion. By solving these equations and comparing the results with the experimental data, the ranges of load carrying capacity with 95% probability are found for different experimental tests.

2. Background on Brownian Motion

In 1828, the Scottish botanist Robert Brown observed irregular movement of pollen suspended in water. As explained by Einstein [14], this random movement is caused by the buffeting of the pollen by water molecules and results in dispersal or diffusion of the pollen in the water. The first mathematically rigorous construction of Brownian motion is credited to Wiener [15], and Brownian motion is sometimes called the Wiener process. Deep studies of Brownian motion and related topics can be found in Øksendal [16].

A real-valued stochastic process $W = \{W(t) : t \geq 0\}$ defined on some probability space (Ω, F, P) is called a standard Brownian motion, if

(i) $W(0) = 0$;

(ii) $W(t)$ has continuous sample paths almost surely;

(iii) for all $0 \leq s < t$, the increment $W(t) - W(s)$ is independent of $F_s := \sigma\{W(u) : 0 \leq u < s\}$ and has Gaussian distribution with: $E[W(t) - W(s)] = 0$, and $E[|W(t) - W(s)|^2] = t - s$.

In the above, E is the mathematical expectation with respect to the probability measure P, and $F_s := \sigma\{W(u) : 0 \leq u < s\}$ is a σ-algebra. One can think F_s as all the information available to the observer by time s. Note that $F_s \subset F_t$ for all $0 \leq s < t$. The collection of σ-algebra $\{F_s\}_{s\geq 0}$ is the natural filtration generated by W. Also, for each $w \in \Omega$, the function $t \to W(t, w)$ can be regarded as a sample path or a realization of the Brownian motion.

In a random experiment, for example, infinite number of coin tossing, the outcome determines the sample path of the Brownian motion. Then $W(t)$ is the value of this path at time t, and this value of course depends on which path resulted from the random experiment. Figure 1 presents five different sample paths of a 1-dimensional standard Brownian motion obtained by using MATLAB.

Even though the Brownian motion W has continuous sample paths, it can be shown that W is nowhere differentiable with probability 1, a mathematical fact explaining the high irregularity of Brownian motion. This means that the derivative of the function $t \to W(t, w)$ does not exist in the ordinary sense for almost all $w \in \Omega$. Still, we may interpret their time derivative in a distributional sense to get a generalized stochastic process called the white noise [16]. White noise generally is a random signal that can be applied to model a totally unpredictable process. It can be considered as the derivative of a Brownian motion existing in the generalized sense. Figure 2 plots a numerical realization of a white noise.

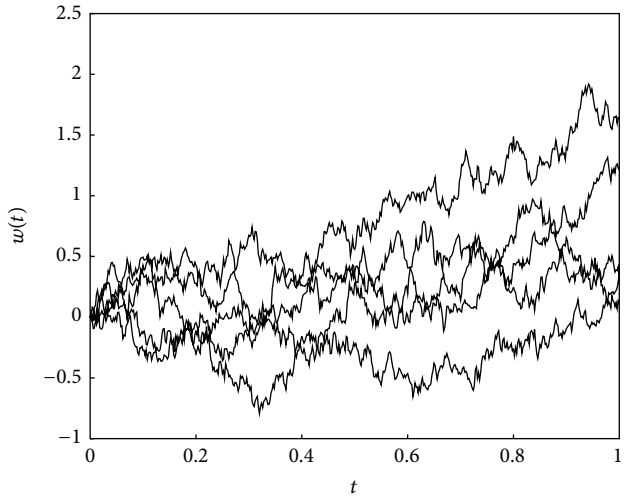

Figure 1: Five sample paths of a 1-dimensional standard Brownian motion.

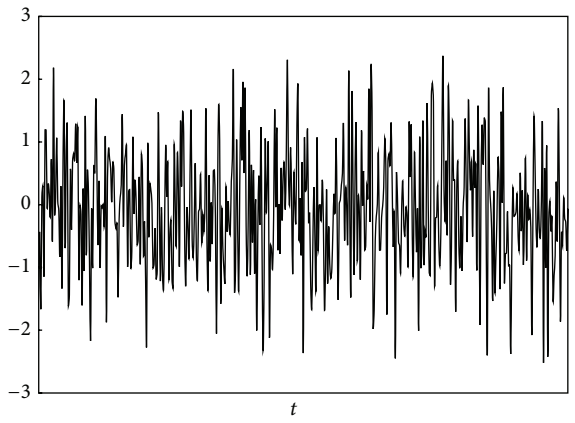

Figure 2: Numerical realization of a white noise.

3. FRP-to-Concrete Interface under Mode II Loading Condition

Figure 3 shows an FRP/concrete interface under a single shear pull-out action; that is, the specimen is subjected to Mode II loading (in-plane shear stress). In this figure, a_0 is the initial crack length between the FRP sheet/plate and the concrete substrate, and a is the new crack length during debonding propagation. As it is already mentioned, experimental studies suggest that the failure of FRP/concrete joints generally occurs in concrete at a few millimetres from the FRP/concrete interface. The ultimate load of the joint therefore depends strongly on concrete failure behaviour.

For a brittle material, the debonding region does not transfer any stresses. Theoretically, there should not be further increasing in load carrying after debonding initiation [4]. For a quasi-brittle material like concrete, the new crack surfaces formed by debonding may be in contact and are tortuous in nature. This leads to toughening mechanisms at the tip of the crack that is taken into account by a conceptual fracture process zone (FPZ). As a result of FPZ, the newly

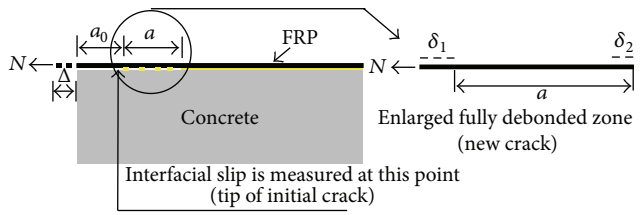

Figure 3: FRP-bonded concrete joint subjected to single shear pull-out (Mode II) force.

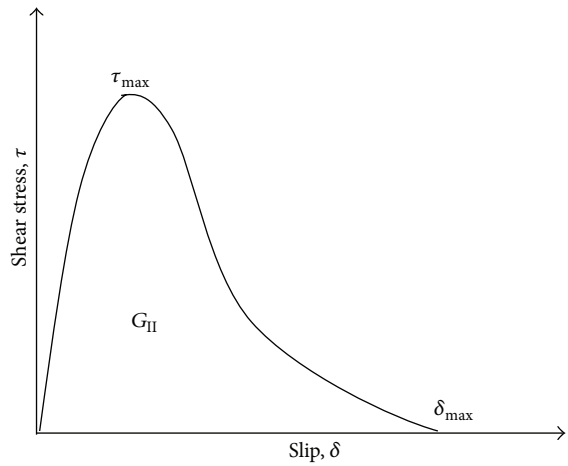

Figure 4: Typical bond-slip behaviour in single shear pull-out test.

formed crack surfaces may continue to sustain more stresses after debonding initiation, which is characterized by a softening branch in a traction-separation relationship [19]. The traction-separation relationship in FRP bonded concrete joints in a single shear pull-out test is known as bond-slip behaviour. Figure 4 shows typical bond-slip behaviour of a single shear pull-out test specimen. Area under the bond-slip curve is considered as required interfacial Mode II fracture energy, $G_{f\mathrm{II}}$, for debonding propagation of FRP from concrete surface subjected to shear stress.

Existing studies indicate that the interfacial fracture energy of FRP/concrete joint is a function of concrete strength and FRP stiffness. Therefore, it is assumed that variation of the interfacial fracture energy can present the variations of concrete strength and FRP stiffness together.

The theoretical ultimate interfacial pull-out force in the FRP sheet, N_u, which is equal to the axial force in FRP, can be expressed as

$$N_u = E_f t_f b_f \varepsilon_{\max}, \tag{1}$$

where E_f is the elastic modulus of FRP; t_f is the thickness of FRP; b_f is the width of FRP sheet; and $\varepsilon_{\max}$ is the maximum strain of FRP sheets corresponding to the maximum pull-out force. On the other hand, the interfacial fracture energy can be calculated by [6]

$$G_{f\mathrm{II}} = \frac{1}{2} E_f t_f \varepsilon_{\max}^2. \tag{2}$$

This relation is independent of bond-slip relation and suitable for any other type of bond-slip models [20]. By substituting (2) into (1), the maximum bearing load is a function of the interfacial fracture energy as shown in the following:

$$N_u = 2G_{f\mathrm{II}} b_f \frac{1}{\varepsilon_{\max}}. \tag{3}$$

Regarding Figure 3, FRP strain at the tip of the initial crack is equal to $\varepsilon = (\delta_1 - \delta_2)/a$, where δ_1 is the interfacial slip at the tip of the initial crack and δ_2 is the interfacial slip at the end of the new crack. When "a" reaches a sufficiently long value "$a_{\max}$", δ_1, which is the elongation of FRP over the fully debonded zone, will be much larger than δ_2, which is the elongation of FRP over the bonded zone. In other words, δ_2 is negligible compared to δ_1. Using this assumption, the FRP strain at the tip of the initial crack is equal to $\varepsilon_{\max} = \delta_{\max}/a_{\max}$, where $\delta_{\max}$ is the maximum interfacial slip at the tip of the initial crack and $a_{\max}$ is the maximum crack length in front of the initial crack corresponding to the ultimate pullout force, N_u, during the interface crack propagation (i.e., macro interface debonding).

By substituting $\varepsilon_{\max} = \delta_{\max}/a_{\max}$ into (3), it can be rewritten as

$$N_u = 2G_{f\mathrm{II}} b_f a_{\max} \frac{1}{\delta_{\max}}. \tag{4}$$

By setting $X = 1/\delta_{\max}$ and $K_0 = 2G_{f\mathrm{II}} b_f a_{\max}$, (4) in differential equation form is

$$\frac{dN_u}{dX} = K_0. \tag{5}$$

Interfacial fracture energy, $G_{f\mathrm{II}}$, is a material property [19] and theoretically it has a constant value. Previous research has shown that "$a_{\max}$" has a fixed relationship with the interfacial fracture energy $G_{f\mathrm{II}}$ [21] and therefore is assumed to be constant in this study. The width of FRP, b_f, can also be considered as a constant. Therefore, $K_0 = 2G_f b_f a_{\max}$ is assumed as a constant in this study.

The interfacial fracture energy is a function of the FRP stiffness and the concrete strength. As discussed in the previous section, the actual FRP tension stiffness achieved *in situ* is not the same as the calculated value. It is inevitably subjected to random fluctuations, resulting from the wet lay-up process and different amount of concrete attached to the debonded FRP at different locations. Also there are some sources for concrete compressive strength variation. In order to find the effect of the FRP tension stiffness and concrete strength variations on the ultimate load carrying capacity (i.e., the maximum pullout load) of the specimens, a white noise is added to the parameter K_0 as in the following:

$$K = K_0 + \alpha \dot{W}, \tag{6}$$

where α is a constant positive value ($\alpha > 0$) that presents the distribution or variation of experimental data, and $\dot{W}$ is a one-dimensional white noise. Since the measured value of δ is a parameter which varies due to the wet lay-up construction process and different amount of concrete attached to the debonded FRP at different locations, $\dot{W}$ is a function of δ (X here). By substituting (6) into (5), the ultimate axial force can be written as

$$dN_u = K_0 dX + \alpha \dot{W} dX. \tag{7}$$

Since white noise can be formally considered as the derivative of a Brownian motion, (7) can be rewritten as

$$dN_u = K_0 dX + \alpha dW(X), \tag{8}$$

where $W(X)$ is a one-dimensional standard Brownian motion. In this application, a Brownian motion is introduced to present the effect of totally unpredictable interfacial fracture energy variation on the load versus deflection responses of the specimens. Equation (8) is a stochastic differential equation and the solution is

$$N_u = K_0 X + \alpha W(X). \tag{9}$$

It is well known that if the random variable ξ has normal distribution with mean μ and variance σ^2, then $(\xi - \mu)/\sigma$ has a standard normal distribution with mean 0 and variance 1 [22]. Recall that if a stochastic process $W = \{W(X),\ 0 \le X < \infty\}$ is a Brownian motion, then W has independent and stationary increments [16], and for each X, $W(X)$ is a normal random variable with mean 0 and variance X. Therefore, $W(X)/\sqrt{X}$ has a standard normal distribution. Then,

$$P\left\{-1.96 < \frac{w(X)}{\sqrt{X}} < 1.96\right\} = 95\%. \tag{10}$$

See Figure 5 for an illustration.

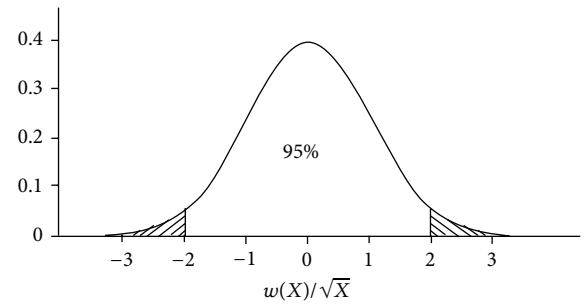

Figure 5: Probability density function for standard Brownian motion.

By substituting (9) into (10), with 95% probability, the upper and lower bounds can be found for the ultimate axial force, N_u, as

$$-1.96 < \frac{N_u - K_0 X}{\alpha\sqrt{X}} < 1.96, \tag{11}$$

$$N_{\mathrm{lower}} = K_0 X - 1.96\alpha\sqrt{X},$$
$$N_{\mathrm{upper}} = K_0 X + 1.96\alpha\sqrt{X}. \tag{12}$$

In (12), the value of constant α, which represents the distribution of experimental data, is needed to determine

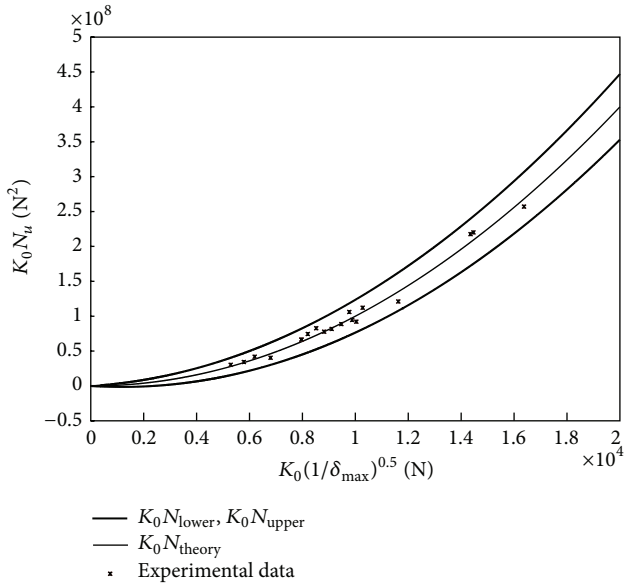

Figure 6: Application of experimental data from Dai et al. [6] to find α.

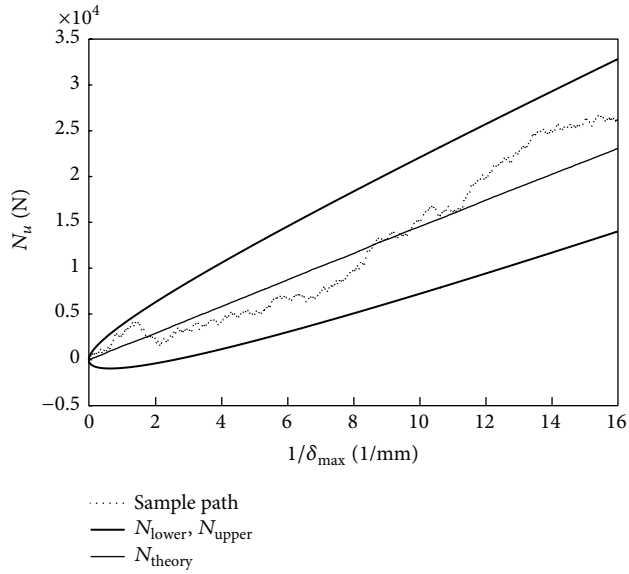

Figure 7: Ultimate load versus maximum slip for specimen CR1L1.

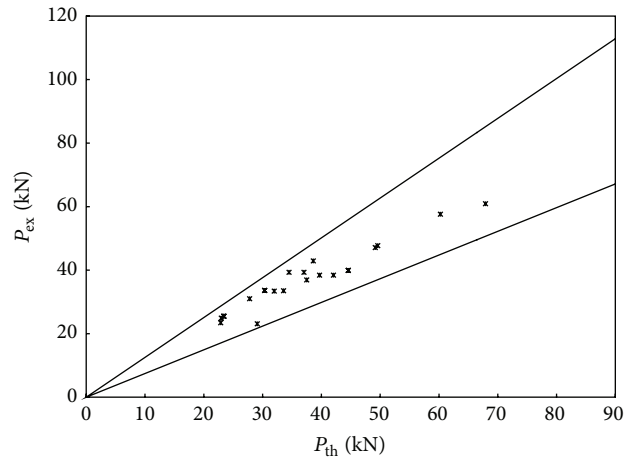

Figure 8: Experimental versus theoretical ultimate loads for the tests by Dai et al. [6].

the lower and upper bounds of the ultimate load. This value has been obtained in this study by using the experimental data from Dai et al. [6].

Table 1 includes the material properties and experimental results of the single shear pullout tests conducted by Dai et al. [6]. The width of the FRP sheets, b_f, is 100 mm. In order to use data from different tests with different materials, normalized K_0N_u against $K_0\sqrt{X}$ curves are drawn in Figure 6. In this figure, the thin line represents the theoretical response calculated from (4), the thick lines are the results from (12), and $*$ points are the experimental data. By adjusting the value of α in (12), the band between the lower and upper N_u values can be changed to involve all experimental data. For these test results, $\alpha = 1200$ is a good estimation to cover the experimental data.

Because N_u is between N_{upper} and N_{lower}, and $\varepsilon_{max} = \Delta_{max}/a_{max}$, using (4) and (12), the bounds of interfacial Mode II fracture energy, $(G_{fII})_{exp}$, with 95% probability can be expressed as

$$\left(G_{fII} - \frac{1.96\alpha\sqrt{1/\delta_{max}}}{2b_f a_{max}}\right) < (G_{fII})_{exp} < \left(G_{fII} + \frac{1.96\alpha\sqrt{1/\delta_{max}}}{2b_f a_{max}}\right). \quad (13)$$

Using $\alpha = 1200$ and (13), the range of Mode II fracture energy bounds has been determined as presented in Table 1. On average, Mode II fracture energies for this group of specimens are within plus or minus 25.4% of the theoretical values.

To give an instance, the ultimate load versus maximum slip for the first specimen in Table 1 (CR1L1) is shown in Figure 7. The thin line is the theoretical one from (4), and the thick lines are the upper and lower bounds of ultimate load based on (12) with $\alpha = 1200$. Due to the Brownian motion, (9) represents a stochastic process, which has many different sample paths. The dashed line in Figure 7 plots one of such sample paths.

Figure 8 shows the experimental ultimate loads (P_{ex}) against the theoretical ones (P_{th}). Because the relationship between the ultimate load and Mode II interfacial fracture energy, G_{fII}, is linear (4), the ultimate bearing load changes 25.4% when the fracture energy changes 25.4%. In Figure 8, the thick lines are the bounds of experimental maximum load versus theoretical one; that is, $P_{ex} = (1 \pm 0.254)P_{th}$. This may explain why the debonding strength of FRP always exhibits quite large scatter [23, 24].

As it can be seen in Figure 8, all experimental ultimate loads are in the bounds. Therefore, it confirms that the proposed method is valid to predict the load capacity variation of the FRP bonded concrete specimens under Mode II loading.

Table 1: Specimens of Dai et al. [6] and their fracture energy bounds.

Specimen	ε_{max}	δ_{max} (mm)	N_u (KN)	Theoretical G_{fII} (N/mm)	G_{fII} lower bound (N/mm)	G_{fII} upper bound (N/mm)	G_{fII} upper and lower bounds away from theoretical G_{fII} (%)
CR1L1	0.00904	0.064	23.4	1.034	0.614	1.454	40.62
CR1L1	0.01046	0.066	23.1	1.384	0.905	1.863	34.70
CR1L1	0.00908	0.053	24.9	1.043	0.579	1.507	44.45
CR1L2	0.00664	0.069	33.5	1.115	0.818	1.412	26.63
CR1L2	0.00682	0.061	39.3	1.177	0.852	1.502	27.61
CR1L2	0.00732	0.077	39.3	1.356	1.046	1.667	22.86
CR1L3	0.00509	0.064	42.9	0.983	0.746	1.212	23.29
CR1L3	0.00554	0.057	38.4	1.165	0.892	1.438	23.43
CR1L3	0.00525	0.062	38.4	1.042	0.794	1.290	23.80
CR1L3	0.00496	0.059	36.9	0.930	0.690	1.170	25.81
AR1L1	0.01260	0.070	25.5	1.476	0.916	2.036	37.94
AR1L2	0.00955	0.073	833.6	1.450	1.034	1.856	28.00
AR1L3	0.00606	0.068	39.9	1.351	1.078	1.624	21.54
GR1L5	0.00732	0.062	33.4	1.171	0.825	1.517	29.54
CR2L1	0.01124	0.111	28.1	1.598	1.201	1.995	24.84
CR2L2	0.00809	0.123	43.2	1.656	1.385	1.927	32.73
CR2L3	0.00596	0.103	47.4	1.343	1.125	1.561	16.23
AR2L3	0.00668	0.111	47.1	1.642	1.406	1.878	14.37
GR2L3	0.00869	0.090	31.0	1.208	0.867	1.548	28.14
CR3L2	0.00980	0.290	47.7	2.430	2.216	2.644	8.80
CR3L3	0.00732	0.227	57.6	2.205	2.024	2.386	8.20
AR3L3	0.00923	0.309	60.9	3.135	2.940	3.330	6.22
						Average (%)	25.4

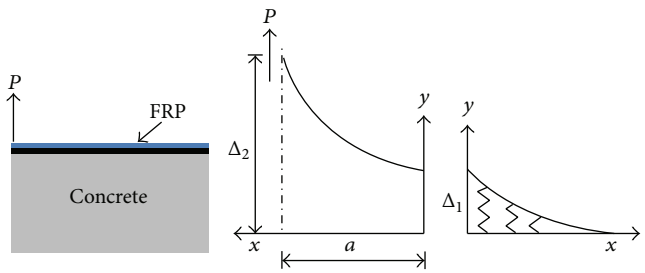

Figure 9: Simulation of FRP on the concrete substrate as a cantilever beam and a beam on elastic foundation for Mode I loading.

4. FRP-to-Concrete Interface under Mode I Loading Condition

The relationship between the load and displacement in a Mode I loading condition can be obtained in a similar way as Mode II loading case. Figure 9 shows the schematic model around the crack tip subjected to a Mode I load, P. If the value of the crack (debonded) length, a, is small, the debonded FRP can be assumed as a cantilever beam subjected to load P, and the bonded parts of FRP can be assumed as an Euler-Bernoulli beam on an elastic Winkler foundation [25, 26]. In this study, the Mode I displacement of the bonded parts of FRP, Δ_1, in Figure 9, is assumed equal to zero because it is very small compared to the displacement at the crack tip, Δ_2. Therefore, the relationship between the ultimate Mode I load, P_u, and the corresponding Mode I displacement, Δ_{max}, can be obtained as

$$P_u = \left[\frac{3EI}{a_{max}^3}\right]\Delta_{max}, \tag{14}$$

where EI is the bending stiffness of FRP and a_{max} is the crack length corresponding to the ultimate load.

Based on the compliance method, the Mode I fracture energy can be expressed as [17, 26]

$$G_{fI} = \frac{P^2}{2b_f}\frac{dC}{da}, \tag{15}$$

where C is the compliance of the unbonded/debonded FRP and can be expressed by

$$C = \frac{\Delta}{P}. \tag{16}$$

Table 2: Specimens of Wan et al. [17] and their fracture energy bounds.

Specimens	P_u (N)	Δ_{max} (mm)	Theoretical G_{fI} (N/mm)	G_{fI} lower bound (N/mm)	G_{fI} upper bound (N/mm)	G_{fI} upper and lower bounds away from theoretical G_{fI} (%)
C4B1S1	515.86	0.58	0.545	0.467	0.622	14.13
C4B1S2	553.09	0.79	0.273	0.191	0.355	30.0
C4B1S3	518.63	0.87	0.417	0.347	0.467	12.0
C4B1S4	545.67	0.98	0.436	0.392	0.480	10.1
C4B1S5	380.97	0.68	0.391	0.342	0.440	12.5
					Average (%)	15.74

Table 3: Specimens of Ouyang and Wan [18] and their fracture energy bounds.

Specimens	P_u (N)	Δ_{max} (mm)	Theoretical G_{fI} (N/mm)	G_{fI} lower bound (N/mm)	G_{fI} upper bound (N/mm)	G_{fI} upper and lower bounds away from theoretical G_{fI} (%)
1	385.4	1.72	0.345	0.181	0.391	13.3
2	260.8	1.45	0.250	0.087	0.312	24.8
3	403.8	1.68	0.229	0.184	0.274	19.6
4	379.9	1.53	0.405	0.388	0.442	9.13
5	420.6	2.06	0.477	0.402	0.552	15.7
6	323.4	1.64	0.422	0.331	0.513	21.5
7	309.8	2.04	0.374	0.306	0.442	18.2
8	411.1	2.15	0.400	0.332	0.468	17.0
					Average (%)	17.4

By substituting (15) and (16) into (14) and setting $K_0 = 2b_f G_{fI} a$ and $X = 1/\Delta_{max}$, the ultimate Mode I load, P_u, can be expressed as

$$P_u = K_0 X. \tag{17}$$

To model the unpredictable changes in the Mode I interfacial fracture energy, G_{fI}, a white noise is added to the parameter K_0, where K_0 is calculated by the manufacturer reported FRP material properties and concrete strength. The process is similar to what has been done for the Mode II loading case. The upper and lower bounds for ultimate Mode I loading, P_u, with probability 95% are

$$\begin{aligned} P_{lower} &= K_0 X - 1.96\alpha\sqrt{X}, \\ P_{upper} &= K_0 X + 1.96\alpha\sqrt{X}. \end{aligned} \tag{18}$$

To find the magnitude of α, experimental data from Wan et al. [17] and Ouyang and Wan [18] are used.

Wan et al. [17] used modified double cantilever beam (MDCB) specimens to test the energy release rate of FRP debonding from concrete subjected to Mode I loading. CFRP sheets were applied to the concrete substrates by wet lay-up process. Ouyang and Wan [18] used the MDCB test to measure the interfacial fracture energy of the CFRP plate debonding from concrete substrate under Mode I loading. The experimental results of these tests are shown in Tables 2 and 3, respectively.

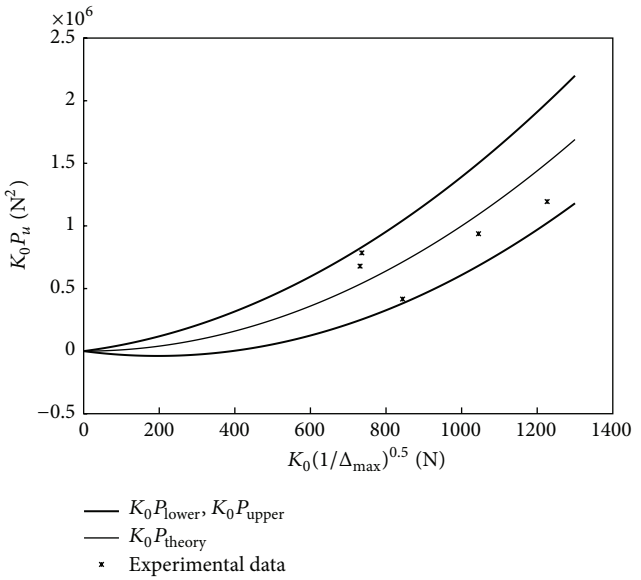

Figure 10: Application of experimental data from Wan et al. [17] to find α.

The normalized K_0P_u against $K_0\sqrt{X}$ curves are drawn in Figure 10 for the specimens in Table 2. The appropriate magnitude for α is equal to 200 to cover all experimental

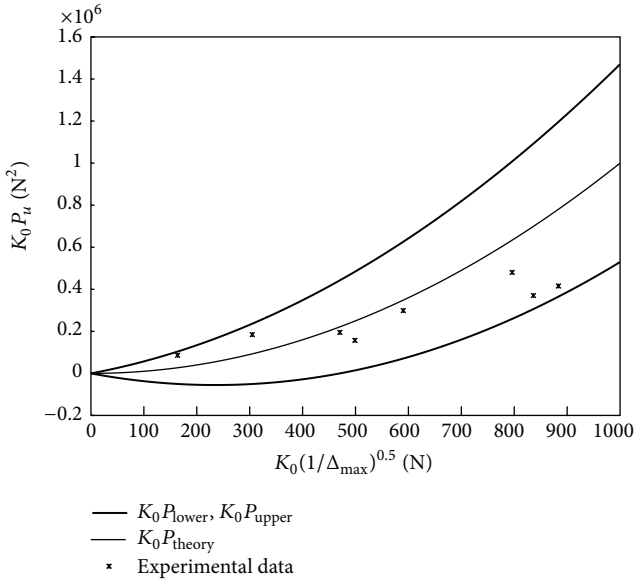

Figure 11: Application of experimental data from Ouyang and Wan [18] to find α.

data in Wan et al. [17]. The α value for experimental data in Ouyang and Wan [18] is equal to 240 as shown in Figure 11.

Because P_u (peak load) is between P_{upper} and P_{lower} at Δ_{max}, using (17) and (18), the bounds of interfacial Mode I fracture energy, $(G_{fI})_{exp}$, with 95% probability can be expressed as

$$\left(G_{fI} - \frac{1.96\alpha\sqrt{1/\Delta_{max}}}{2b_f a_{max}}\right) < (G_{fI})_{exp} < \left(G_{fI} - \frac{1.96\alpha\sqrt{1/\Delta_{max}}}{2b_f a_{max}}\right). \quad (19)$$

By using (19) and the obtained values of α, the range of the bounds of the Mode I interfacial fracture energy has been determined for the experimental data, and they are presented in Tables 2 and 3. It can be seen that, on average, the variations of the actual fracture energies of the specimens tested by Wan et al. [17] are within plus or minus 15.7% of the theoretical values, while it is 17.4% for the specimens tested by Ouyang and Wan [18].

According to (17), the relationship between ultimate bearing load and interfacial Mode I fracture energy is linear. Figure 12 shows the experimental ultimate load against analytical ones for specimens in Wan et al. [17] and Ouyang and Wan [18]. In this figure, the thick lines are bounds of experimental maximum load versus theoretical one; that is, $P_{ex} = (1 \pm 0.174)P_{th}$. As it can be seen, all experimental ultimate loads are within the bounds. Therefore, it confirms that the proposed method can predict the load capacity variation of the specimens subjected to Mode I loading.

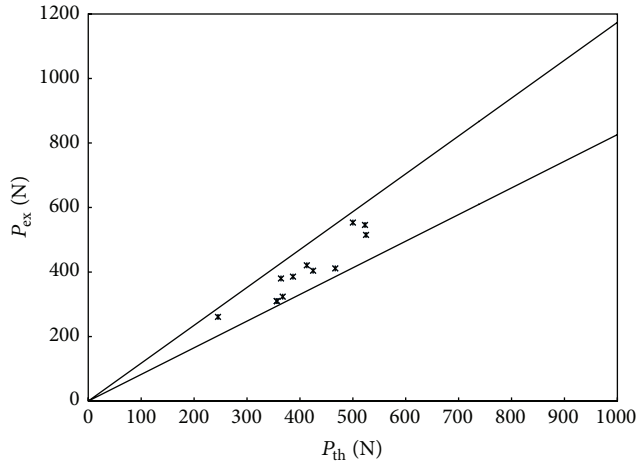

Figure 12: Experimental ultimate load versus theoretical ones for the tests by Wan et al. [17] and Ouyang and Wan [18].

5. Conclusion

In this study, white noise and Brownian motion are introduced to model the variation of interfacial fracture energy in FRP bonded concrete specimens subjected to Mode I and Mode II loadings. A systematic method is developed to determine the range of interfacial fracture energy and load carrying capacity. Experimental data from literatures are used to demonstrate the validity of this methodology. For the experimental data used in this research, Mode I and Mode II load carrying capacities are within ±17.4% and ±25.4%, respectively, of their theoretical values.

Conflict of Interests

The authors declare that there is no conflict of interests regarding the publication of this paper.

Acknowledgments

This study was supported by the financial aid for graduate student research assistant from Marquette University Graduate School. The research of Chao Zhu was supported in part by the National Science Foundation under DMS-1108782 and a grant from the UWM Research Growth Initiative.

References

[1] C. E. Bakis, L. C. Bank, V. L. Brown et al., "Fibre-reinforced polymer composites for construction, state—of-the-Art Review," *Journal of Composites for Construction*, vol. 6, no. 2, pp. 73–87, 2002.

[2] L. Hollaway and M. B. Leeming, *Strengthening of Reinforced Concrete Structures: Using Externally-Bonded FRP Composites in Structural and Civil Engineering*, Woodhead Publishing, 1999.

[3] ACI Commitee 440.2R-08, *Guide for the Design and Construction of Externally Bonded FRP Systems for Strengthening Concrete Structures*, American Concrete Institute, Farmington Hills, Mich, USA, 2008.

[4] H. Yuan, J. G. Teng, R. Seracino, Z. S. Wu, and J. Yao, "Full-range behavior of FRP-to-concrete bonded joints," *Engineering Structures*, vol. 26, no. 5, pp. 553–565, 2004.

[5] X. Z. Lu, J. G. Teng, L. P. Ye, and J. J. Jiang, "Bond–slip models for FRP sheets/plates bonded to concrete," *Engineering Structures*, vol. 27, no. 6, pp. 920–937, 2005.

[6] J. G. Dai, T. Ueda, and Y. Sato, "Development of the nonlinear bond stress-slip model of fiber reinforced plastics sheet–concrete interfaces with a simple method," *Journal of Composites for Construction*, vol. 9, no. 1, pp. 52–62, 2005.

[7] S. S. Shams and R. F. El-Hajjar, "Effects of scratch damage on progressive failure of laminated carbon fiber/epoxy composites," *International Journal of Mechanical Sciences*, vol. 67, pp. 70–77, 2013.

[8] S. S. Shams and R. F. El-Hajjar, "Overlay patch repair of scratch damage in carbon fiber/epoxy laminated composites," *Composites Part A: Applied Science and Manufacturing*, vol. 49, pp. 148–156, 2013.

[9] O. Buyukozturk and B. Hearing, "Failure behavior of precracked concrete beams retrofitted with FRP," *Journal of Composites for Construction*, vol. 2, no. 3, pp. 138–144, 1998.

[10] J. F. Chen and J. G. Teng, "Anchorage strength models for FRP and steel plates bonded to concrete," *Journal of Structural Engineering*, vol. 127, no. 7, pp. 784–791, 2001.

[11] C. A. Coronado and M. A. Lopez, "Experimental characterization of concrete-epoxy interfaces," *Journal of Materials in Civil Engineering*, vol. 20, no. 4, pp. 303–312, 2008.

[12] J. K. Wight and J. G. MacGregor, *Reinforced Concrete: Mechanism and Design*, Pearson Education, Upper Saddle River, NJ, USA, 6th edition, 2012.

[13] J. G. MacGregor and F. M. Bartlett, *Reinforced Concrete: Mechanism and Design*, Pearson Education, Toronto, Canada, 1st edition, 1999.

[14] A. Einstein, "On the movement of small particles suspended in stationary liquids required by the molecular-kinetic theory of heat," *Annalen der Physik*, vol. 17, pp. 549–560, 1905.

[15] N. Wiener, "Differential spaces," *Journal of Mathematical Physics*, vol. 58, pp. 131–174, 1923.

[16] B. Øksendal, *Stochastic Differential Equations: An Introduction with Applications*, Springer, Berlin, Germany, 6th edition, 2003.

[17] B. Wan, M. A. Sutton, M. F. Petrou, K. A. Harries, and N. Li, "Investigation of bond between fiber reinforced polymer and concrete undergoing global mixed mode I/II loading," *Journal of Engineering Mechanics*, vol. 130, no. 12, pp. 1467–1475, 2004.

[18] Z. Ouyang and B. Wan, "Experimental and Numerical study of water effect on bond fracture energy between FRP and concrete in moist environments," *Journal of Reinforced Plastics and Composites*, vol. 27, no. 2, pp. 205–223, 2008.

[19] S. P. Shah, S. E. Swartz, and C. Ouyang, *Fracture Mechanics of Concrete: Applications of Fracture Mechanics to Concrete, Rock, and Other Quasi-Brittle Materials*, John Wiley & Sons, New York, NY, USA, 1995.

[20] J. G. Dai and T. Ueda, "Local bond stress relations for FRP sheets-concrete interfaces," in *Proceeding of the 6th International Symposium on FRP Reinforcement for Concrete Structures*, pp. 143–152, World Scientific Publications, Singapore, July 2003.

[21] J. Dai, T. Ueda, and Y. Sato, "Unified analytical approaches for determining shear bond characteristics of FRP-concrete interfaces through pullout tests," *Journal of Advanced Concrete Technology*, vol. 4, no. 1, pp. 133–145, 2006.

[22] P. Billingsley, *Probability and Measure*, John Wiley & Sons, New York, NY, USA, 2nd edition, 1986.

[23] C. Mazzotti, M. Savoia, and B. Ferracuti, "An experimental study on delamination of FRP plates bonded to concrete," *Construction and Building Materials*, vol. 22, no. 7, pp. 1409–1421, 2008.

[24] H. Toutanji, M. Han, and E. Ghorbel, "Interfacial bond strength characteristics of FRP and RC substrate," *Journal of Composites for Construction*, vol. 16, no. 1, pp. 35–46, 2012.

[25] J. Pan and C. K. Y. Leung, "Debonding along the FRP-concrete interface under combined pulling/peeling effects," *Engineering Fracture Mechanics*, vol. 74, no. 1-2, pp. 132–150, 2007.

[26] J.-G. Dai, B.-L. Wan, H. Yokota, and T. Ueda, "Fracture criterion for carbon fiber reinforced polymer sheet to concrete interface subjected to coupled pull-out and push-off actions," *Advances in Structural Engineering*, vol. 12, no. 5, pp. 663–682, 2009.